OPTOGENETICS

Optogenetic stimulation of cochlear neurons activates the auditory pathway and restores auditory-driven behavior in deaf adult gerbils

Christian Wrobel[1,2,3]*†, Alexander Dieter[1,4,5]*, Antoine Huet[1,5]‡, Daniel Keppeler[1,4]‡, Carlos J. Duque-Afonso[1,4], Christian Vogl[2,6], Gerhard Hoch[1,2,5], Marcus Jeschke[1,5]§, Tobias Moser[1,2,4,5,7,8]§

Cochlear implants partially restore hearing via direct electrical stimulation of spiral ganglion neurons (SGNs). However, spread of excitation from each electrode limits spectral coding. We explored the use of optogenetics to deliver spatially restricted and cell-specific excitation in the cochlea of adult Mongolian gerbils. Adeno-associated virus carrying the gene encoding the light-sensitive calcium translocating channelrhodopsin (CatCh) was injected into the cochlea of adult gerbils. SGNs in all cochlea turns showed stable and long-lasting CatCh expression, and electrophysiological recording from single SGNs showed that light stimulation up to few hundred Hertz induced neuronal firing. We characterized the light-induced activity in the auditory pathway by electrophysiological and behavioral analysis. Light- and sound-induced auditory brainstem responses showed similar kinetics and amplitude. In normal hearing adult gerbils, optical cochlear implants elicited stable optical auditory brainstem responses over a period of weeks. In normal hearing animals, light stimulation cued avoidance behavior that could be reproduced by subsequent acoustic stimulation, suggesting similar perception of light and acoustic stimuli. Neurons of the primary auditory cortex of normal hearing adult gerbils responded with changes in firing rates with increasing light intensity. In deaf adult gerbils, light stimulation generated auditory responses and cued avoidance behavior indicating partial restoration of auditory function. Our data show that optogenetic cochlear stimulation achieved good temporal fidelity with low light intensities in an adult rodent model, suggesting that optogenetics might be used to develop cochlear implants with improved restorative capabilities.

INTRODUCTION

About 360 million people suffer from disabling hearing impairment (HI) (*1*). HI hampers communication and often causes social isolation, depression, and reduction in professional capabilities. Sensorineural HI is the most common form of hearing loss; it results from cochlear dysfunction or degeneration typically involving loss of sensory hair cells. Hearing aids and electrical cochlear implants (eCIs) provide partial restoration of hearing for sensorineural HI. The eCI bypasses dysfunctional or lost cochlear hair cells via direct electric stimulation of spiral ganglion neurons (SGNs) and provides most of about 500,000 users with open speech comprehension (*2*–*4*). One of the goals of current CI research is to increase the coding of spectral information that is very limited in eCIs because of wide spread of current around each electrode contact (*5*). The resulting channel cross-talk limits the number of useful frequency channels to less than 10 and explains why eCI users suffer from poor speech comprehension in noisy environments. Increasing the frequency resolution of coding has been explored using multipolar stimulation, intraneural electrodes, engineered outgrowth of neurites toward eCI contacts, and stimulation by optical CI (oCI) (*6*–*12*).

A first proof-of-principle study on optogenetic SGN stimulation used transgenic mice and rats and prenatal adeno-associated virus (AAV)–mediated gene transfer to mouse SGNs and demonstrated activation of the auditory pathway up to the inferior colliculus and a lower spread of cochlear excitation for fiber-based oCI than for monopolar eCI (*12*). However, much remains to be carried out to further develop, characterize, and optimize oCIs on their way toward potential clinical translation. Critically, a postnatal approach for manipulating SGNs across all cochlear turns needs to be established. Moreover, although oCI has been shown to improve frequency resolution compared to eCI, this seemed to be traded in for poorer temporal fidelity of oCI coding (*12*). Higher temporal fidelity of oCI coding might be achieved by using faster channelrhodopsins (ChRs) such as Chronos, which has already been tested for optogenetic stimulation of the auditory brainstem, or the recently developed ChR2 variant CatCh (calcium translocating ChR). CatCh seems to support rapid repolarization due to enhanced Ca^{2+} influx recruiting more large conductance Ca^{2+}-activated K^+ channels and might thus be of interest for oCI coding (*13*–*16*). Finally, although mice and rats are often the species of choice in preclinical studies, testing oCI in other species with a hearing system more closely resembling human condition is critical to understand the translational potential of oCIs.

Here, we established AAV-mediated expression of CatCh in SGNs of adult Mongolian gerbils and characterized optogenetic stimulation by electrophysiology and behavioral analysis. The gerbil is of particular interest for preclinical studies of oCI because, in contrast to other rodents, its hearing extends to the low frequency range used by the human ear

[1]Institute for Auditory Neuroscience and InnerEarLab, University Medical Center Göttingen, 37075 Göttingen, Germany. [2]Collaborative Research Center 889, University of Göttingen, 37075 Göttingen, Germany. [3]Department of Otorhinolaryngology, Head and Neck Surgery, Ruhr University Bochum, St. Elisabeth Hospital, 44787 Bochum, Germany. [4]Göttingen Graduate School for Neurosciences and Molecular Biosciences, University of Göttingen, 37075 Göttingen, Germany. [5]Auditory Neuroscience and Optogenetics Group, German Primate Center, 37077 Göttingen, Germany. [6]Presynaptogenesis and Intracellular Transport in Hair Cells Group, Institute for Auditory Neuroscience and InnerEarLab, University Medical Center Göttingen, 37075 Göttingen, Germany. [7]Bernstein Center for Computational Neuroscience, University of Göttingen, 37077 Göttingen, Germany. [8]Center for Nanoscale Microscopy and Molecular Physiology of the Brain, University of Göttingen, 37075 Göttingen, Germany.
*These authors contributed equally to this work.
†Present address: Department of Otorhinolaryngology and InnerEarLab, University Medical Center Göttingen, 37075 Göttingen, Germany.
‡These authors contributed equally to this work.
§Corresponding author. Email: marcus.jeschke@med.uni-goettingen.de (M.J.); tmoser@gwdg.de (T.M.)

and its cochlea is relatively large (only about 2.5-fold smaller than the human cochlea). We demonstrate that optogenetically driven activity achieves good temporal fidelity. Using chronic oCIs, we show the reliability of optogenetic stimulation over weeks and find that it potently cues avoidance behavior. We characterize the response of single neurons of the auditory cortex to oCI stimulation. Finally, we show that oCI restores some auditory function in a gerbil model of ototoxic deafness.

RESULTS

Optogenetic manipulation of the adult spiral ganglion via direct modiolar AAV-CatCh injection

We first tested the transfection properties of Chronos and CatCh using various administration routes in adult gerbils (fig. S1A). Compared to the strong abundance of CatCh in the plasma membrane of SGNs, Chronos showed a more intracellular expression pattern and did not evoke optically evoked auditory brainstem responses (oABRs) (fig. S1, B and C); therefore, we decided to use AAV2/6 carrying CatCh linked to the reporter protein enhanced yellow fluorescent protein (eYFP) under control of the human synapsin promoter for injections into the modiolus of adult gerbils (8 to 19 weeks of age; Fig. 1A). We adapted a retroauricular approach previously used to graft neural precursor cells (*17*). We approached the spiral ganglion from the bulla using a fine dental file bypassing the scala tympani to inject 2 to 3 µl of AAV-CatCh suspension (Fig. 1, B to D).

The number of SGNs and their expression of CatCh-eYFP were analyzed by confocal microscopy of immunolabeled midmodiolar cryosections 4 to 12 weeks after injection in animals that showed

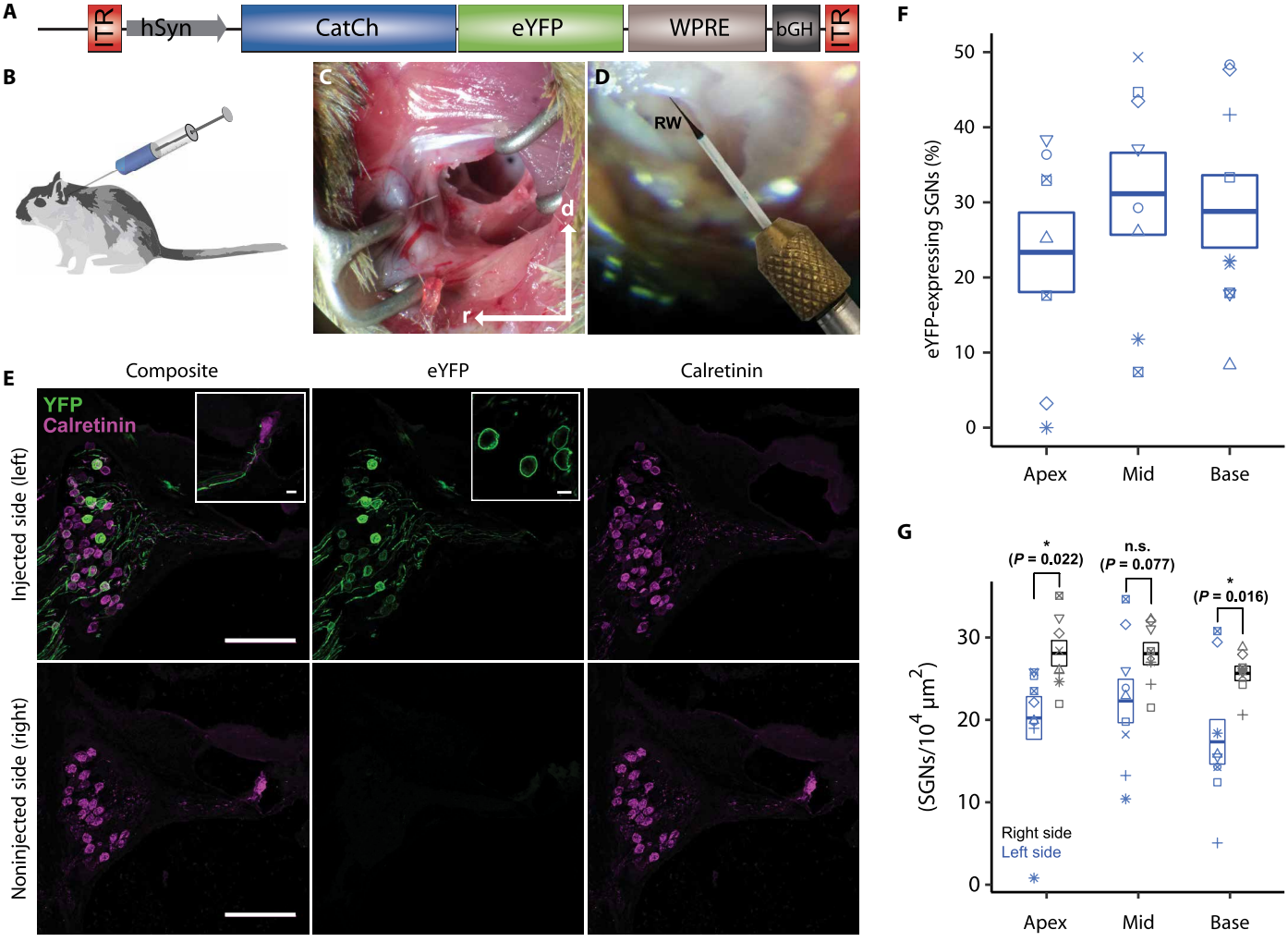

Fig. 1. AAV-CatCh–mediated optogenetic manipulation of cochlear SGNs in adult gerbils. (**A**) Scheme of the AAV construct used to transduce SGNs with CatCh-eYFP. hSyn, human synapsin promoter. (**B**) Depiction of retroauricular injection of the AAV-CatCh. (**C**) Photo of the retroauricular approach to the middle ear of a gerbil (r, rostral; d, dorsal): The bullostomy provides a view into the middle ear. (**D**) Montage of images showing the round window (RW) niche and dye-filled glass capillary, which points to the manually drilled hole. (**E**) Confocal images of immunolabeled midmodiolar cochlear cryosections (representative section of a middle turn) of an AAV-CatCh–injected adult gerbil. eYFP (green) marks transduced SGNs, and calretinin (magenta) generically marks SGNs. Scale bars, 100 µm. It should be noted that the apparent abundance of CatCh in the cytoplasm results from the maximum projection as individual *z* sections demonstrates a clear membrane expression. Inset (top left): Calretinin-positive but eYFP-negative IHC (arrowhead), with associated eYFP-positive, peripheral SGN neurites. Scale bar, 10 µm. Inset (top center): Close-up single *z* section of SGNs, highlighting the apparent plasma membrane expression of the construct. Scale bar, 10 µm. (**F**) Box plot showing the fraction of eYFP-expressing SGNs for the apical, middle, and basal cochlear turn of the injected left ear. No expression was found in the noninjected right ear ($n = 9$). (**G**) Box plot showing SGN density for the apical, middle, and basal cochlear turn of the injected left ear and the noninjected right ear ($n = 9$; $^*P < 0.05$, *t* test). Data in (F) and (G) are shown as mean ± SEM. n.s. not significant. ITR, inverted terminal repeat; bGH, bovine growth hormone derived polyadenylation site; WPRE, woodchuck hepatitis virus posttranscriptional regulatory element.

functional response to optical stimulation (46%, 44 of 96 injected animals). CatCh-eYFP expression was limited to SGNs of the injected ear, which showed prominent labeling in the plasma membrane of somata and neurites all the way to the inner hair cells (IHCs; Fig. 1E). SGNs of all three cochlear turns (apex, mid, and base) were transduced to a similar extent (on average, about 30%; Fig. 1F). A mild loss of SGNs across all turns was observed in the injected cochlea (about 25%, significant in comparison with the right noninjected side, $P < 0.001$; Fig. 1G). A similar extent of SGN loss was also found in AAV-CatCh–injected ears that largely lacked CatCh expression (about 35 %, significant in comparison to the right noninjected side, $P = 0.006$), suggesting that the SGN loss likely resulted from damage caused by the pressure injection into the fixed volume of Rosenthal's canal housing the SGNs (fig. S2).

Characterization of optical activation of the auditory pathway by auditory brainstem responses

To characterize the light-induced activation of the auditory pathway, we first recorded oABRs using fiber-coupled laser stimulation 4 to 12 weeks after AAV-CatCh injection (Fig. 2A). Blue light stimulation through a cochleostomy in the middle cochlear turn or through the round window evoked oABRs in AAV-CatCh–injected animals (Fig. 2B and fig. S3). Optical stimulation induced one to four peaks in the ABR, which likely reflected the synchronous activation of CatCh-expressing SGNs (first peak) and the downstream auditory pathway (subsequent peaks). oABR amplitudes varied between animals and were positively correlated with the fraction of CatCh-expressing SGNs (fig. S4, A and B). Increasing light intensity resulted in increased oABR amplitude [quantified by the difference between the first positive (p1) and negative peak (n1)] and decreased the latency to response [Fig. 2, C and D; quantification for the second positive and negative peak (p2-n2) is shown in fig. S4, C and D]. Although the average threshold of acutely measured oABRs amounted to 4.6 mW (±2.8 mW; $n = 14$), stimuli as weak as 1 to 2 mW (duration, 1 ms; rate, 10 Hz; 1 to 2 μJ per pulse) were sufficient to drive oABRs in some animals. In 8 of 20 animals, oABR amplitudes increased with light intensity rising over more than an order of magnitude. The response did not plateau in the majority of animals (75% without a plateau) such that we could only approximate an apparent dynamic range from the stimulus amplitude functions, which amounted to 16.02 ± 6.14 dB. The latency of the first oABR peak was 0.95 ± 0.17 ms. Analyzing oABR in response to different stimulus durations, we found that oABRs could be elicited by stimuli as short as 200 μs (fig. S4, E and F). Analysis of the dependence of oABRs on the stimulus rate (duration, 1 ms; intensity, 21 to 32 mW) showed that increasing stimulus rate reduced oABR amplitude and prolonged latency; however, oABRs remained sizable up to stimulus rates of at least 200 Hz (Fig. 2, E to G, and fig. S4, G and H).

Quantitative comparison of acoustically evoked ABR (aABR) from unrelated, noninjected gerbils and oABR data with the highest laser intensity possible at our setup (~30 mW) showed similar amplitudes with clicks of 40-dB peak equivalent sound pressure level (SPL), whereas larger amplitudes of aABRs evoked by clicks of 50 to 70 dB exceeded those of oABRs (Fig. 2, H to J, and fig. S5A). Latencies of oABRs were significantly shorter than for aABRs evoked by clicks even at 80-dB SPL ($P < 0.0001$; fig. S5B).

p1-n1 amplitude declined, and p1 latency increased with increasing stimulation rate for both oABR and aABR (Fig. 2, L and M). To evaluate the magnitude of the effect of stimulation rate on ABR amplitude, we measured the p1-n1 amplitude ratio measured at 150-Hz over 10-Hz stimulation rate. For aABR, the ratio amounted to 0.39 ± 0.15, indicating a 2.5-fold reduction (mean ± SD; $n = 13$ gerbils). For oABR, the ratio was 0.67 ± 0.37, indicating a 1.5-fold reduction (mean ± SD; $n = 20$ gerbils). Together, these results suggest that the CatCh-mediated optogenetic coding achieves a temporal fidelity similar to that of acoustic coding on the neural population level.

Electrophysiological characterization of optical activation of single SGNs

To further validate the CatCh-mediated SGN stimulation and scrutinize the temporal fidelity of stimulation, we performed juxtacellular recordings in vivo from individual SGNs during blue light stimulation from an optical fiber inserted through the round window (*18*). To maximize the chances to record SGNs, we inserted the electrode under visual control directly into the auditory nerve. At 10 Hz, 20 of 29 SGNs fired one spike to each laser pulse; the remaining nine SGNs responded with multiple spikes (2.6 ± 0.68 spikes per pulse), suggesting the presence of two separable clusters of SGNs (Fig. 3, A and B). The first spike elicited by each pulse in a 10-Hz train was significantly more synchronized to the stimulus for the SGNs responding with a single spike (jitter, 0.26 ± 0.49 ms) than for the multiple spike–responding SGNs (jitter, 1.66 ± 1.49 ms; $P \leq 0.01$; Fig. 3C). Raster plots and peristimulus time histogram in response to light pulse trains of 10, 100, and 300 Hz are shown for both a representative single spike (Fig. 3, D to F) and a representative multiple spike unit (Fig. 3, G to I). Light pulses triggered spikes with substantial temporal precision as evident from high vector strength (0.85 ± 0.07) up to a stimulus rate of 100 Hz (Fig. 3J). At higher repetition rates, vector strength dropped to 0 for most SGNs and remained low but significant in some SGNs (average vector strength for all SGNs above their cut-off frequencies: 0.1 ± 0.06; $P < 0.001$; Rayleigh test). The vector strength of non-transduced SGNs in response to acoustic click trains revealed phase-locked responses up to the highest tested rate (500 Hz; Fig. 3J, black dashed line, and fig. S6). The highest frequency leading to synchronized responses to optical stimulation was 100 Hz for most of the single spike–responding SGNs (Fig. 3K). On average, the maximal frequency eliciting synchronized responses to optical stimulation was significantly higher for multiple spike–responding SGNs (242.8 ± 127.2 versus 121.4 ± 57.7 Hz, $P \leq 0.001$; Fig. 3L). In contrast, optogenetically driven single spike–responding SGNs increased their discharge rate up to 100 Hz, followed by a drop to ~0 spikes/s at higher rates, whereas multiple spike–responding SGNs also sustained the response for higher rates (Fig. 3M). Above 100 Hz, the discharge rate of multiple spike–responding SGNs to light pulse trains was comparable to acoustic click trains (Fig. 3M, black dashed line). At repetition rates of ≥100 Hz, single spike–responding SGNs preferentially showed phasic responses (adaptation ratio, ≥10; $n = 12$ of 15 cells), whereas multiple spike–responding SGNs fired in a tonic fashion (adaptation ratio, <10; $n = 9$ of 9 cells; Fig. 3N). These recordings directly demonstrate optogenetic SGN excitation and corroborate the ABR results indicating substantial temporal fidelity with optogenetic stimulation.

Chronic oCI development and electrophysiological characterization

To study a possible percept elicited by optogenetic SGN stimulation, we developed and implanted a chronic fiber-based single-channel oCI in gerbils 4 to 8 weeks after AAV-CatCh or phosphate-buffered saline (PBS only) injection (Fig. 4A). Functionality of the oCI was

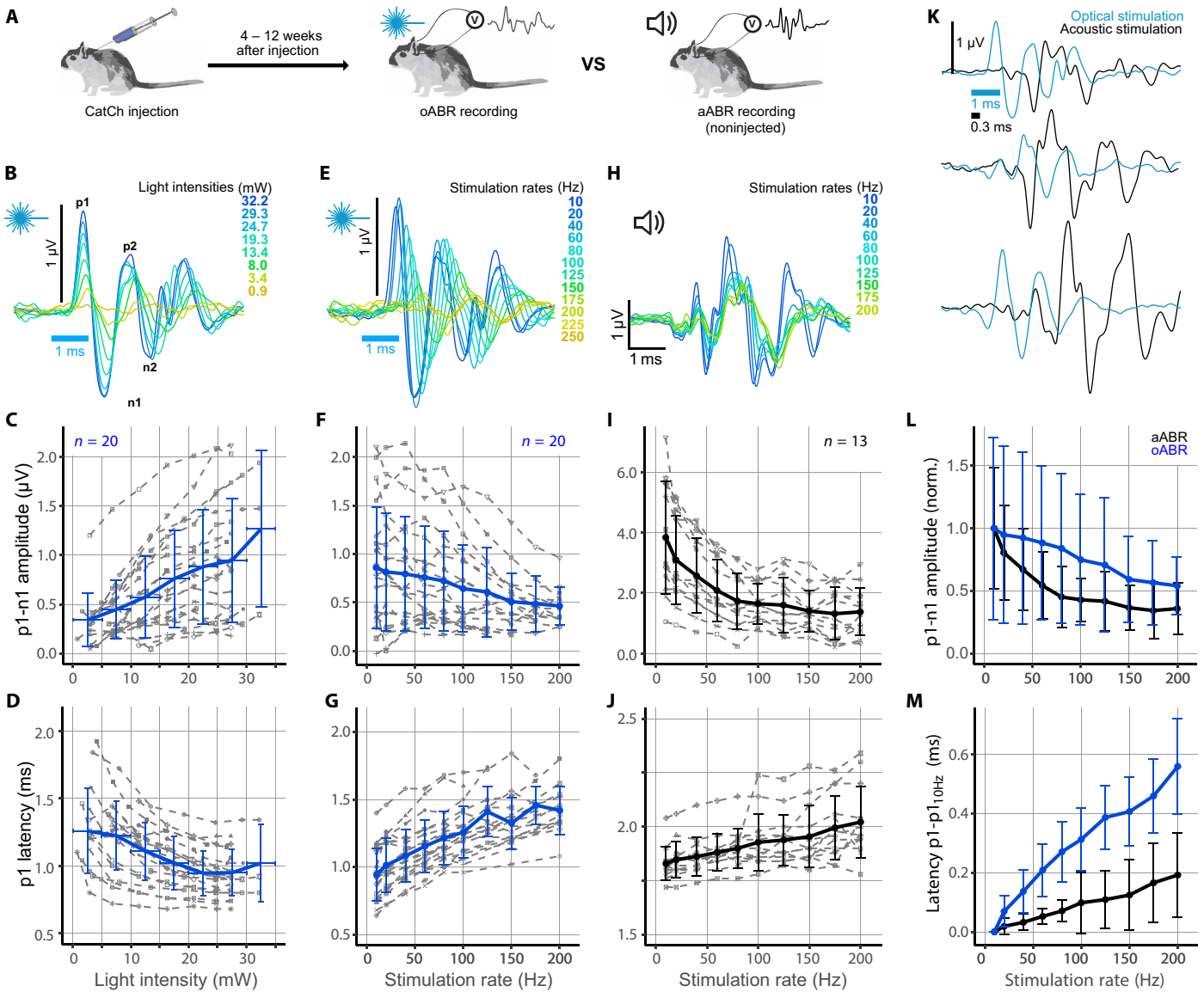

Fig. 2. Characterization of optical and acoustic ABR in gerbils. (**A**) Experimental workflow: 4 to 12 weeks after AAV-CatCh injection, oABRs were recorded and compared to aABRs of the same gerbils and to those of noninjected animals. Light of a 473-nm laser was coupled in by a 200-µm optical fiber via cochleostomy on the middle cochlear turn or through the round window. (**B**) oABRs from a representative AAV-CatCh–injected adult gerbil with varying light intensities (radiant flux, 1 ms at 10 Hz). Colors code the stimulus parameters. (**C**) Amplitude of oABR p1-n1 as a function of light intensity (1-ms light pulses at 10 Hz). (**D**) Latency of oABR p1 as a function of light intensity for the same 20 gerbils (gray) as in (C). (**E**) oABRs from a representative AAV-CatCh–injected adult gerbil with varying stimulus rates (32.2 mW for 1 ms). (**F**) Amplitude of oABR p1-n1 as a function of stimulus rate (1-ms light pulses with high light intensities of 21 to 32 mW). (**G**) Latency of oABR p1 as a function of stimulus rate for the same 20 gerbils (gray) as in (F). Gray lines in (C), (D), (F), and (G) symbolize different animals ($n = 20$), and blue line represents mean with vertical error bars indicating SD. Horizontal error bars in (C) and (D) represent the SD of the mean light intensity in the respective bin. (**H**) aABRs (80-dB SPL, 0.3 ms) recorded at increasing acoustic click stimulation rate. (**I**) Quantification of aABR ($n = 13$) p1-n1 amplitude as a function of stimulation rate for acoustic clicks. Gray lines symbolize different animals; black line represents mean with vertical error bars indicating SD. (**J**) aABR p1 latency plotted against stimulation rate of auditory clicks ($n = 13$). (**K**) oABRs (blue; 32.2 mW, 1 ms at 10 Hz) and aABRs (black; click of 0.3 ms, 70 dB, at 10 Hz) recorded in three representative AAV-CatCh–injected adult gerbils. (**L**) p1-n1 amplitude as a function of stimulus rate normalized against p1-n1 amplitude of 10-Hz aABRs (black) and oABRs (blue); data are shown as mean ± SD. (**M**) Latency of p1 as function of stimulation rates normalized against p1 latency of 10 Hz aABRs (black) and oABRs (blue) (mean ± SD). Data in (C), (D), (F), (G), (L), and (M) are pooled for oABR measurements in acutely and chronically implanted animals.

monitored by regular oABR recordings (every other day during the first week after surgery and once a week afterward), eliciting stable responses in AAV-CatCh–injected but not PBS-injected animals [AAV-CatCh, $n = 7$; PBS, $n = 5$ (two of these five animals have been implanted and measured chronically); Fig. 4B]. Chronic oCI produced stable and reliable responses more than 3 weeks in all gerbils. Two animals were continuously tested until after behavioral experiments and showed stable responses for more than 100 days (Fig. 4C). oABR amplitudes were similar between the last day of behavioral testing and the day after surgery (1.33 ± 0.86 µV after

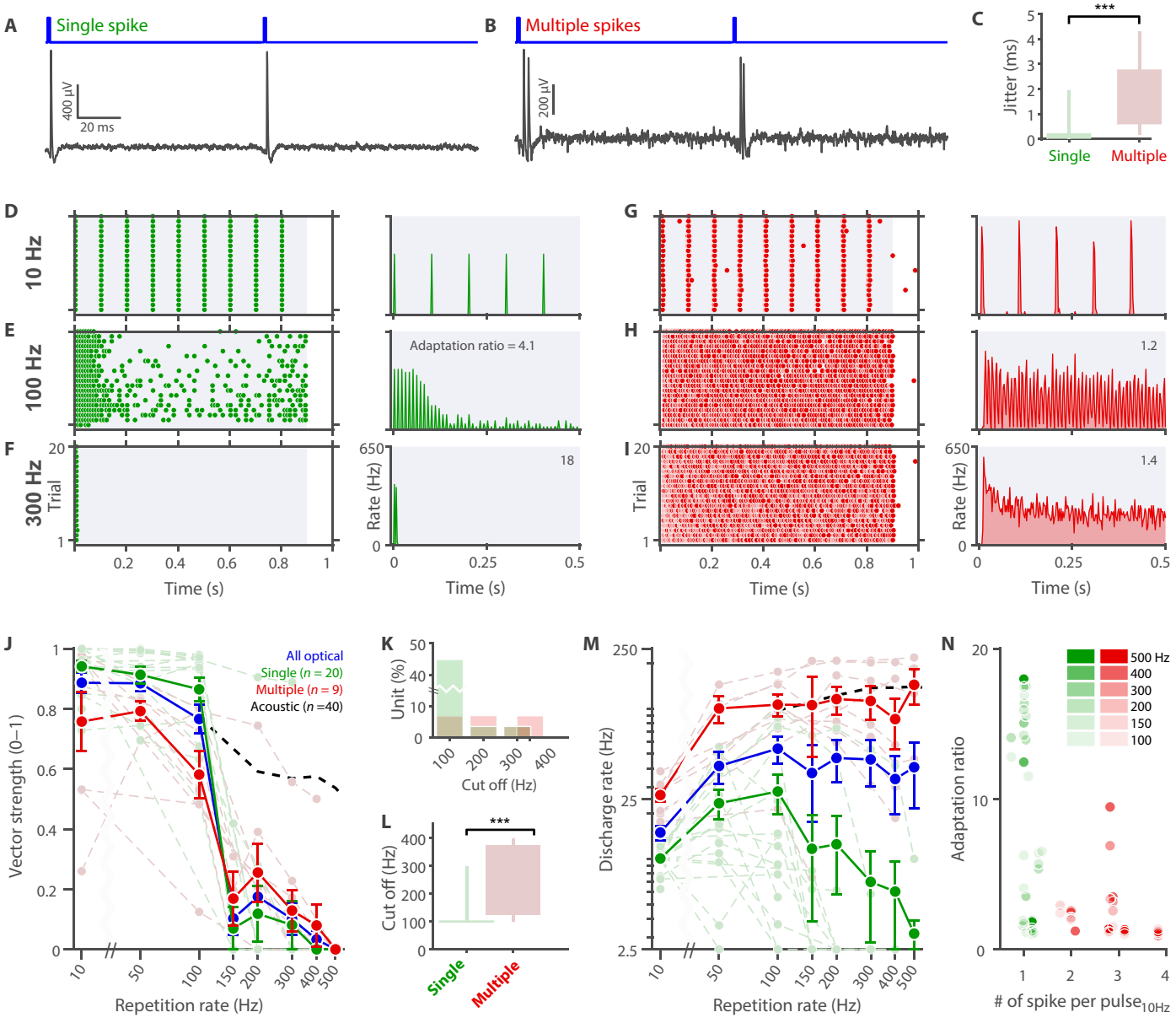

Fig. 3. Characterization of SGN responses to optogenetic stimulation. (**A** and **B**) Representative juxtacellular SGN recordings during the first 200 ms of a 900 ms pulse train (1 ms, 20 mW) with a repetition rate of 10 Hz of an exemplary single spike–responding (A) and a multiple spike–responding (B) SGN. (**C**) Quantification of the first spike jitter elicited per light pulse for single spike–responding (green) and multiple spike–responding (red) SGNs. (**D** to **I**) Raster plots and peristimulus time histogram of a single spike–responding (D to F) and a multiple spike–responding (G to I) SGN in response to 900-ms train pulses of 10, 100, and 300 Hz. (**J**) Vector strength as a function of repetition rate ($n = 29$). Blue lines correspond to the population mean, green lines to single spike–responding SGNs, red lines to multiple spike–responding SGNs, and dashed black line to acoustic stimulation of control SGN (see fig. S4 for details). (**K** and **L**) Distribution (K) and quantification (L) of the cutoff frequency (highest frequency with a significant vector strength) for single spike–responding (green) and multiple spike–responding (red) SGNs. (**M**) Discharge rate as a function of repetition rate ($n = 29$). (**N**) Adaptation ratio as a function of the number of spikes per light pulse in response to 10-Hz light pulse train. A color scale is used to represent the repetition rate. Data are expressed as mean ± SEM, and the statistical difference between groups were tested by Mann-Whitney *U* test (***$P \leq 0.001$).

surgery, 0.99 ± 0.42 µV after behavioral testing, $P = 0.14$; $n = 7$), indicating a largely stable physiological response over time (fig. S7A). The mean oABR threshold 24 hours after chronic oCI surgery was 6.9 ± 2.46 mW and was significantly elevated compared to oABRs measured in acute experiments [4.6 ± 2.8 mW; $n = 7$ (for chronic) and 14 (for acute measurements); $P = 0.038$; fig. S7, B and C]. However, thresholds decreased over time, and 3 weeks after implantation, the responses were comparable to acute experiments (4.7 ± 2 mW, $P = 0.44$; fig. S7C). The position of the implanted fiber relative to the spiral ganglion was investigated with x-ray tomography of the cochlea (*19*). In these studies on five postmortem specimen, the aperture always pointed slightly off the central axis of the modiolus (Fig. 4D and fig. S8). Therefore, the optical fiber was not optimally orientated toward the SGNs.

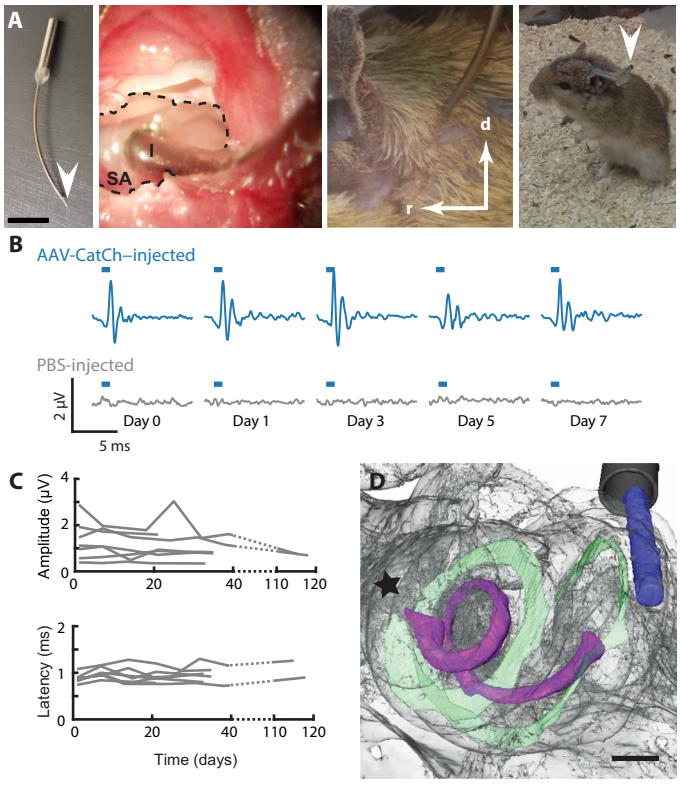

Fig. 4. Chronic fiber-based, single-channel oCI. (**A**) Left: Chronic fiber-based single-channel oCI (arrow) housed in a stainless steel capillary. Scale bar, 1 cm. Center left: oCI (l) placed through the round window into the scala tympani just above the stapedial artery (SA). Dashed line represents bullostomy. Center right: oCI 3 weeks after surgery. Right: Gerbil 3 days after implantation. Arrowhead indicates ferrule for optical fiber connection. (**B**) oABRs of a AAV-CatCh–injected animal (top) at the day of implantation (day 0), and 1, 3, 5, and 7 days after implantation, no oABR was found in PBS-injected animals (bottom). Blue bars indicate optical stimuli. (**C**) oABR amplitudes (p1-n1; top) and latencies (p1; bottom) during the course of behavioral experiments ($n = 7$ up to day 40 after implantation; two animals to day 115); each line corresponds to a single animal. (**D**) X-ray tomography of the cochlea including implant to confirm the fiber's position after behavioral experiments. Green, basilar membrane; purple, Rosenthal's canal; black, steel capillary; blue, optical fiber; star, cochlear apex. Scale bar, 500 μm.

Behavioral assessment of chronic oCI

To test whether the electrophysiological responses triggered by optical stimulation had functional effects on behavior, we chose the shuttlebox paradigm of negative reinforcement learning (Fig. 5, A to C). The test has been successfully used for auditory studies in gerbils and uses mild electrodermal stimulation of the paws to reinforce crossing a barrier to a safe compartment upon a sensory target stimulus (*20*). To adapt the animals to the arena without risk of damage to the oCI, we performed one session with acoustic click trains (Fig. 3D). This session was followed by subsequent optogenetic training. Gerbils learned to react to optogenetic stimuli over roughly a week, typically reaching more than 80% hit rate on day 6 of the daily training program (Fig. 5E). Spontaneous crossing during nontarget trials (interspersed trials without cue stimuli and negative reinforcement) occurred in typically 20% of these trials. Our results showed that learning strictly required opsin expression by SGNs: Response rates for target and nontarget trials did not differ in PBS-injected animals, although they were stimulated with relatively strong light pulses (10 ms × 30 mW = 300 μJ). Hit rates of AAV-CatCh–injected animals broke down upon blocking the light path in the ferrule (still producing light emission at the coupler but not in the cochlea itself) and were restored immediately after reopening the path, suggesting that the behavioral responses were not induced by visual cuing (the blue light emission at the coupler) or by other sensory cues (Fig. 5F). Optogenetically trained gerbils transferred the avoidance behavior to acoustic stimulation: Hit rates in acoustic stimulation sessions were comparable to hit rates using optogenetic stimulation from the first acoustic session on, and two of five tested gerbils crossed the barrier to the safe compartment already in response to the first acoustic stimulus, suggesting at least some degree of generalization between the percepts elicited by optogenetic and acoustic stimulation (Fig. 5G).

After basic shuttlebox training, we estimated behavioral thresholds for light intensity and duration of the laser pulses. Here, within one session, target trials of either different light intensities or different pulse durations, as well as nontarget trials, were presented pseudo-randomly. After six identical sessions (60 repetitions of each trial type), for each light intensity and pulse duration, we compared the hit rate of individual animals for each stimulus condition to the hit rate of nontarget trials in the same animal ($P < 0.01$). Testing different light intensities ranging from 0.1 to 25 mW, we found that the hit rate dropped sharply below 1.8 mW on average (1.8 μJ per pulse; Fig. 5, I and J). This is below the thresholds obtained for acute recordings of oABR (4.6 μJ; see above) and single-neuron responses in auditory cortex (3.11 μJ; see below). The average threshold for stimulus duration was about 140 μs (individual thresholds for four of five animals were as short as 50 μs; Fig. 5, K and L).

Neuronal response properties in primary auditory cortex and cochlear spread of excitation

In an effort to further characterize the auditory signaling elicited by oCI, we performed in vivo extracellular recordings from layer IV of the contralateral primary auditory cortex (AI) while stimulating the AAV-CatCh–transduced SGNs at the base of the cochlea with blue light (Fig. 6A). When an AI neuron was isolated, we first mapped its best frequency (BF; sound frequency for which the maximal spike rate was obtained). BFs progressed to higher frequencies along electrode tracks and covered the tonotopic range (Fig. 6B). A total of 43 neurons in AI were studied of which 38 responded to pure tones with frequencies in the hearing range of gerbils. Among these, 20 neurons responded to optogenetic SGN stimulation (1-ms pulse length and about 1-Hz repetition rate) albeit at different thresholds. Among the total set of 43 neurons studied, 22 responded to individual light pulses.

A range of response types was found: Most of the neurons showed monotonically increasing firing rates with growing light intensity, whereas the firing rate of other neurons first rose but then decreased upon further enhancing light intensity (nonmonotonic response; monotonicity index, <0.5; Fig. 6, C and D). Neurons with high BF (8 to 32 kHz) had a mean threshold of 1.4 ± 1.0 mW (SD; $n = 5$) consistent with the oABR and behavioral thresholds. Thresholds of lower BF neurons (1 to 8 kHz) were significantly higher (8.0 ± 9.5 mW; $n = 12$; $P = 0.046$), indicating that limited light spread in the cochlea occurs (Fig. 6E and fig. S9).

We followed up the aspect of light spread within the cochlea by a Monte Carlo ray tracing model based on an x-ray imaged gerbil cochlea with the 200-μm optical fiber implanted into scala tympani via the round window (fig. S10A). We modeled 3 million rays (λ = 473 nm)

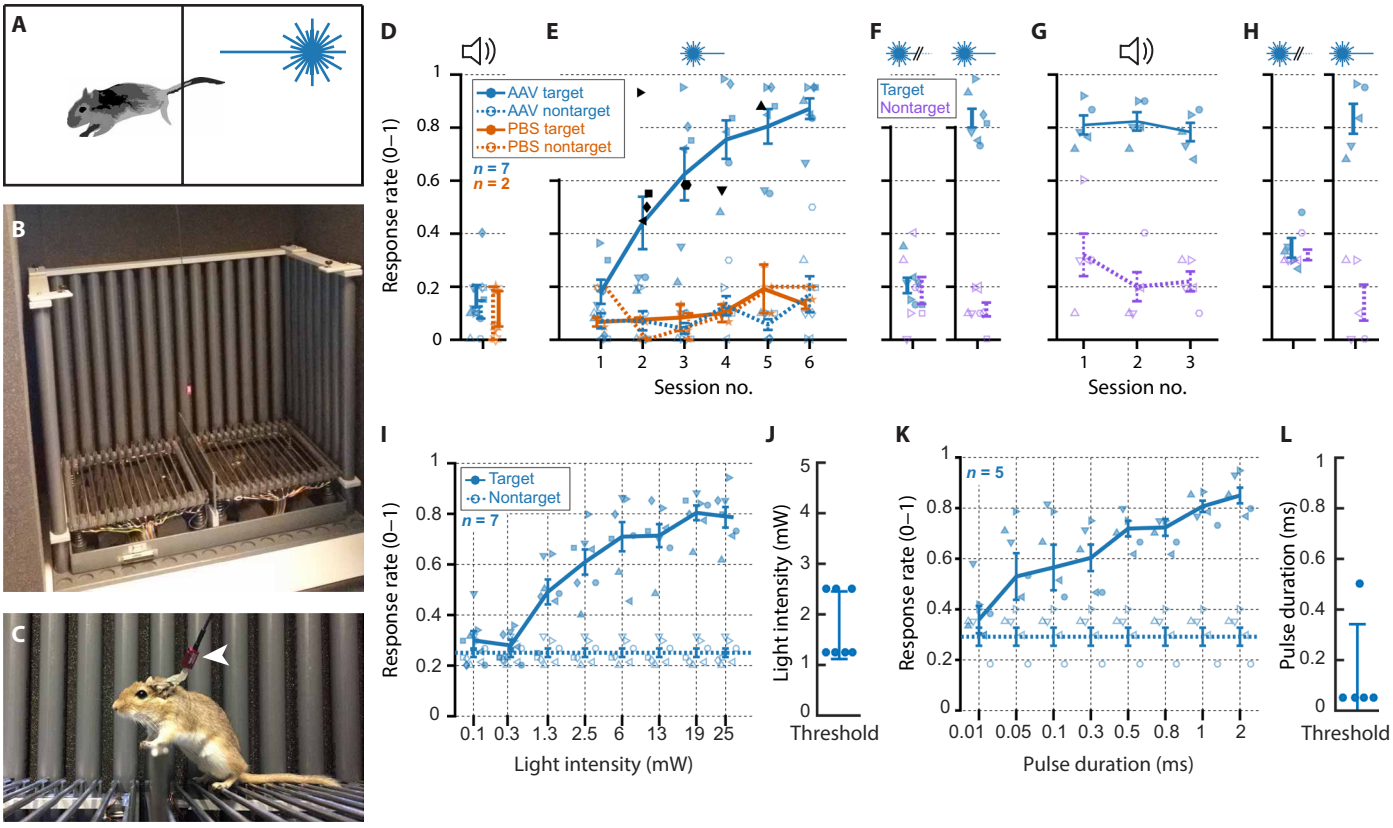

Fig. 5. Optogenetically cued avoidance behavior. (**A**) Outline of the task: After an initial training period, the gerbil changes the compartments of the shuttlebox upon stimulus presentation (acoustic or optogenetic). (**B** and **C**) Picture of the shuttlebox (front wall removed) in a sound-attenuating chamber (B) and of a gerbil in the setup (C). Arrowhead indicates the interface between ferrule and optical fiber. (**D** and **E**) Behavioral performance during the course of shuttlebox training for a single habituation session using acoustic stimuli (D) and the subsequent training period using optogenetic stimulation (E). Solid and dashed lines show mean response rates for target and nontarget trails ± SEM for AAV-CatCh–injected (blue; $n = 7$) and PBS-injected (orange; $n = 2$) animals. Filled and empty markers show response rates for target and nontarget trails, respectively, for each individual animal. (**F**) Response rates in response to target (blue) and nontarget (purple) trials during a control experiment with a blocked (left) and reopened (right) beam path. (**G**) Transfer from optogenetic to acoustic cues for avoidance behavior. (**H**) Second control performed after transfer to acoustic stimulation. Different marker shapes correspond to different animals and are consistent throughout the figure. (**I** to **L**) Average hit rates and behavioral thresholds of individual animals for light power (I and J) and pulse duration (K and L). Solid and dashed lines indicate mean response rates for target and nontarget trails ± SEM across all animals [$n = 7$ (I) and 5 (K)]. Filled and empty markers show hit rates for target and nontarget trials, respectively. Behavioral thresholds were defined as the weakest stimuli eliciting significant performance in each individual animal (chi-square test, $P < 0.01$).

to investigate the spread of excitation at the center of Rosenthal's canal, where the somata of SGNs are housed. With a fiber output of 1 mW (chosen from the thresholds for most sensitive neurons recorded in AI in the range around 10 kHz), we estimated the threshold for neuronal excitation in Rosenthal's canal to be 0.06 mW/mm^2 and the bandwidth of excitation to range from 10 to 14.7 kHz (0.56 octaves; fig. S10, B and C). As expected, we observed an increased light spread with fiber outputs of 5 and 10 mW that reached superthreshold irradiances at cochlear regions with BFs of 5.7 to 26.3 kHz (2.2 octaves) and 3.05 to 32.1 kHz (3.4 octaves), respectively (fig. S9, B and C). For these stronger light intensities, additional peaks of excited SGNs were observed: 0.51 to 0.87 (5 mW) and 0.39 to 1.34 kHz (10 mW; fig. S10, B and C). We note that the projection of light from the round window does not represent the appropriate optical stimulation strategy for a future oCI.

Therefore, we also modeled the spread of excitation for light delivered by a small optical fiber (10 µm of diameter with a 0.1 numerical aperture) as an ideal light emitter placed at four different locations in the center of scala tympani along the tonotopic axis each facing Rosenthal's canal that houses the SGN somata (fig. S10D). Our simulations revealed narrow light spread and indicated that excitation of distinct populations of SGNs can be achieved using optogenetic stimulation at emitter intensities in the range of microwatts (fig. S10, E and F).

Hearing restoration in a gerbil model of ototoxic deafness

Finally, we explored the potential of chronic oCI for restoring hearing in a gerbil model of ototoxic deafness. After measuring aABRs, AAV-CatCh–injected gerbils were trained to detect 70-dB click trains using the shuttlebox paradigm. Animals were then deafened by bilateral, intracochlear injections of kanamycin (2 µl of 100 mg/ml) (*21*). Deafness was confirmed by the absence of aABR (up to the highest SPL amenable to our sound system (110-dB SPL) and the inability to perform shuttlebox behavior with acoustic stimulation (Fig. 7A).

We then implanted single-channel oCIs and demonstrated optogenetic activation of the auditory pathway by means of oABR (Fig. 7, B and C). Post hoc immunofluorescence analysis indicated the absence of hair cells from kanamycin-deafened ears (Fig. 7D). oABR

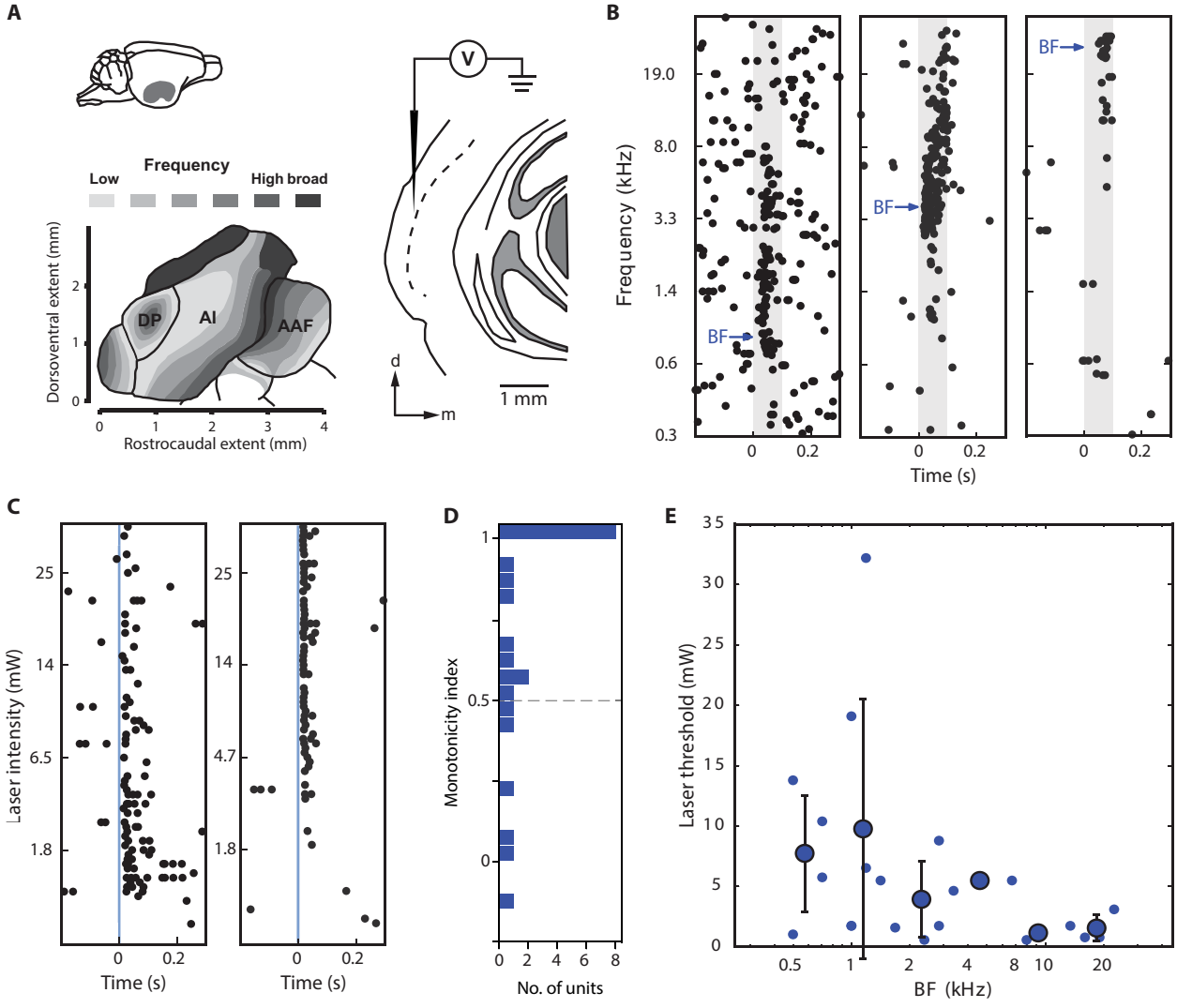

Fig. 6. Responses of single AI neurons to optogenetic SGN stimulation. (**A**) Schematic shows the experimental approach: After initial mapping of the tonotopic representation to identify field AI of the contralateral auditory cortex, a single tungsten electrode was tangentially inserted and advanced to study the activity of single AI neurons (single unit) within the thalamorecipient layer IV. (**B**) Neuronal responses of three individual neurons to pure tones along a representative recording track. The BFs of neurons varied systematically along each electrode track where BFs were lower dorsally and increased ventrally. (**C**) Neuronal responses to individual laser pulses (1 ms at 1 Hz) applied to the contralateral cochlea in a nonmonotonic (left) and monotonic unit (right). (**D**) Distribution of monotonicity indices of all recorded units. Dashed bar indicates a monotonicity index of 0.5 to discriminate between nonmonotonic and monotonic units. (**E**) Comparison of acoustic and optical response properties. BFs are plotted against the corresponding laser threshold for each single unit ($n = 20$). AAF, anterior auditory field; DP, dorsoposterior field; d, dorsal; m, medial.

thresholds of kanamycin-treated chronically implanted gerbils were comparable to kanamycin-untreated chronically implanted gerbils (mean ± SD, 7.9 ± 3.5 mW; $n = 4$ in treated animals; mean ± SD, 6.9 ± 2.4 mW; $n = 7$ in untreated animals). Next, we tested whether these acoustically trained animals, which could not use acoustic cueing any longer upon deafening, could transfer the learned behavior or would (re)learn the behavior by the optogenetic stimulation (Fig. 7, E to G). One of the four gerbils tested, immediately crossed to the safe compartment upon the first optogenetic stimulation with a final hit rate of more than 80%, suggesting transfer of the acoustically cued behavior to the optogenetic cue; the other animals learned to use the optogenetic cue within a few days. On average, acoustically pretrained and kanamycin-treated oCI implanted gerbils took 2.0 days (±0.8 SD; $n = 4$) to relearn the task using an optical cue compared to 3.5 ± 1.7 days ($n = 4$; not different) when learning the task using acoustic stimulation in naive animals. As expected, the deafened gerbils could no longer use the acoustic cue even at the highest SPL amenable to our shuttlebox system (100-dB SPL; Fig. 7H). In conclusion, oCI stimulation of SGNs restored activation of the auditory pathway in a gerbil model of human ototoxic deafness as revealed by analysis of physiological and behavioral responses.

DISCUSSION

Here, we established the Mongolian gerbil as a rodent model for developing the oCI. We achieved AAV-mediated expression of CatCh in cochlear SGNs of adult Mongolian gerbils and characterized optogenetic stimulation by electrophysiology of single neurons and

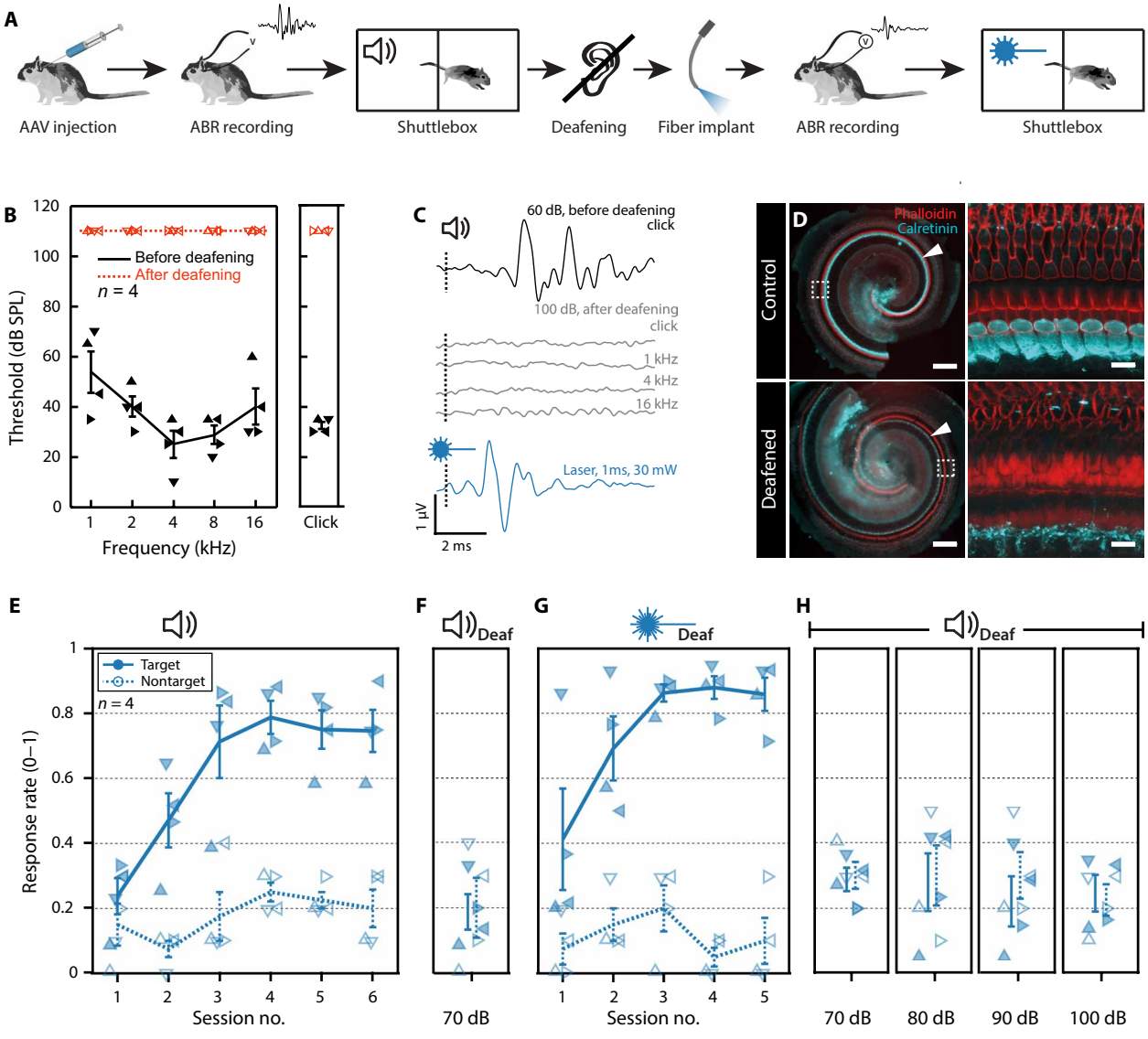

Fig. 7. Restoration of hearing in a gerbil model of ototoxic deafness. (**A**) Experimental workflow: After AAV-CatCh injection, ABRs were recorded, and gerbils were trained in the shuttlebox for 6 days using acoustic stimulation and finally deafened by bilateral intracochlear injections of Kanamycin solution. After deafness was confirmed using aABRs and a single shuttlebox session, animals were implanted with an optical fiber. Subsequently, oABRs were recorded, and shuttlebox experiments were performed using optogenetic stimulation. (**B**) aABR thresholds (individual data and mean ± SEM, $n = 4$) for logarithmically spaced pure tones ranging from 1 to 16 kHz and click stimuli, before (black triangles and solid line) and after deafening (red triangles and dashed line). (**C**) Representative aABR in response to a 60-dB click stimulus before deafening (black; top.). Absence of aABRs in response to 100-dB click stimuli and 1, 4, and 16 kHz pure tones after deafening (gray; middle). oABRs in AAV-CatCh–injected oCl-implanted deafened animal (blue; bottom). Vertical dashed lines indicate stimulus onsets. All traces were recorded from the same animal. (**D**) Histological verification of IHC loss upon deafening. Overview of the apical turn of the organ of Corti in a control animal (top left) and a kanamycin deafened animal (bottom left). Phalloidin was used to stain actin prominently expressed in hair cells and supporting cells (red), and calretinin was used to stain SGNs and IHCs (cyan): Arrowheads point to the location of IHCs. Note the lack of IHCs in the deafened animals. Scale bars, 100 µm. Right: Magnification of the regions outlined on the left side, respectively. Note that spiral ganglion afferents are still present in the deafened animal (bottom right). Scale bar, 10 µm. Learning curves of shuttlebox behavior using 70-dB acoustic stimulation before deafening (**E**), 70 dB after deafening (**F**), optogenetic cues (**G**), and acoustic cues up to 100 dB after deafening (**H**). Solid and dashed lines indicate the mean hit rates ± SEM for target and nontarget trials, respectively. Filled and empty markers indicate the individual rates for each animal ($n = 4$). Different marker shapes correspond to different animals and are consistent throughout the figure.

neural populations and by behavioral analysis. CatCh-mediated optogenetic SGN stimulation drove the auditory pathway up to the AI and elicited avoidance behavior. Intramodiolar AAV-CatCh injection achieved CatCh expression in about 50% of the injected cochleae, where about 30% of the SGNs were transduced. We did not find evidence for viral spread beyond the injected ear. All three cochlear turns were transduced to a similar extent, which contrasts the primarily basal expression obtained with transuterine AAV injection (*12*). The injection caused loss of SGNs (25%) that is likely to be due to the pressure injection, as it was also found in AAV-CatCh–injected ears where no opsin expression was observed. Because calretinin is thought to stain a subset but not all SGNs, the use of calretinin staining

for identification of SGNs might have caused an underestimation of the number of SGNs and an overestimation of the transduction rate (*22*). Hence, despite calretinin labeling the vast majority of SGNs in our experience, future studies should use more global neuronal markers to indiscriminately label all SGNs, such as β-III tubulin (*23*). Nonetheless, despite the relatively low SGN transduction rate in the present study, we obtained electrophysiological and behavioral responses in adult CatCh-positive gerbils. The finding that oABR could already be elicited when 10% of the SGNs were transduced contrasts our previous study in which at least 40% of the transduced SGNs were needed to support optophysiological responses (*12*).

In contrast to the very large (10 to 100 s of microvolt) and delayed (3 ms) optically evoked far-field potentials reported for transgenic mice and rats, we observed smaller and earlier potentials with targeted viral optogenetic manipulation of the ear of gerbils (*12*). These differences might be due to a more localized expression of CatCh in SGNs using injections into the adult spiral ganglion, compared to the Thy1.2-driven broad neuronal expression of ChR2 used in our previous work that might have resulted in optogenetic stimulation extending to structures beyond the auditory pathway. In support of this hypothesis, here, oABRs and aABRs were more similar in amplitude and showed the expected short latency for direct optogenetic SGN stimulation. oABRs remained sizable for stimulus rates of up to 200 Hz, and the oABR amplitude reduction of 1.5-fold observed when raising stimulus rate from 10 to 150 Hz, was favorable compared to the aABR amplitude reduction (2.5-fold), indicating that temporal fidelity of optogenetic coding might approach near physiological performance. We consider this an important advance over our previous work, which indicated much lower temporal fidelity (responses were only found up to 70 Hz) (*12*). Our juxtacellular recordings from single SGNs confirmed specific, synchronized optogenetic excitation of SGNs up to repetition rate of 100 Hz for all recorded fibers. This result supports the temporal fidelity reported by oABR and is in accordance with the closing kinetic of CatCh (16 ms measured at room temperature) (*14*). The lower spike precision and limited spike probability at stimulus rates beyond 100 Hz observed are likely compensated at the neuronal population level, as several SGNs jointly encode information from each place of the tonotopic map (*24*).

We found considerable differences in oABR amplitudes among the gerbils. This variability might be due to differences in transduction rate, amount of CatCh expression among the transduced cells, and positioning of the optical fiber. Nonetheless, the key features such as the dependence of p1-n1 amplitude and p1 latency on the radiant flux and rate of stimulation were comparable among different CatCh-transduced animals. We could not determine the exact light propagation from the fiber aperture within the cochlea, and hence, it was not possible to determine the precise irradiance at a given point of the SGNs. However, we used a Monte Carlo ray tracing model to estimate the irradiance at the site of neural excitation. Considering the maximum light intensity used in our behavioral experiments (30 mW), we estimate the maximal irradiance at the site of SGN somata to be about 2 mW/mm^2, which is within the safe range for optogenetic in vivo applications (up to ~75 mW/mm^2 for 0.5 to 50 ms pulses; even up to ~300 mW/mm^2 in some studies) (*25*, *26*). Furthermore, the oABR long-term stability for >100 days observed here suggests absence of tissue damage due to optogenetic stimulation.

In 40% (8 of 20) of the tested animals oABR increased in amplitude when increasing light intensity more than one order of magnitude, indicating an output dynamic range of optical coding >20 dB. Because the response did not plateau in most animals, the average apparent dynamic range of 16 dB is likely an underestimation. This contrasts with coding with eCI where typically <10-dB dynamic range was reported (*4*). This might reflect the lower spread of excitation with optical stimulation and differences in the expression of CatCh among SGNs at the tonotopic place of stimulation. Recordings of oABR revealed a minimal stimulus duration of <200 μs and an energy threshold of about 4.6 μJ per pulse. Recordings of single-neuron firing in AI confirmed this energy threshold. A recent study in awake primates demonstrated that about 40% of neurons in the auditory cortex could be driven by contralateral eCI stimulation (*27*), whereas we observed 52% of neurons driven by oCI in the gerbil.

Our chronic experiments used a fiber-based single-channel oCI that enabled stable stimulation over several weeks. This allowed longitudinal tracking of oABR and behavioral analysis of oCI function in individual gerbils. The absence of learning by PBS-injected animals rules out the sensation of optothermal or optoacoustic effects in the cochlea as a behavioral cue. In AAV-CatCh–injected gerbils, behavioral estimates of thresholds for light pulse intensity and duration were lower than those obtained in our oABR experiments, indicating that activation of few neurons might suffice to trigger SGN stimulation. Still, behavioral experiments might have overestimated the energy threshold of oCI because postmortem x-ray phase contrast tomography of the implanted cochlea indicated nonoptimal projection to the spiral ganglion from the fiber. Therefore, the behavioral estimate of the energy threshold (2 μJ) is lower than the threshold obtained with physiological methods but might still overestimate the light required for triggering auditory perception.

Nonetheless, lowering the energy requirement, which currently exceeds the energy per pulse in eCI (0.2 μJ for biphasic pulses of 80 μs), remains an important objective to fully capitalize on the potential of oCI for miniaturizing the stimulation site [for example, using 50-μm-sized light-emitting diodes (LEDs) compared to hundreds of micrometer for eCI], to avoid potential phototoxicity and thermal effects, and to enable acceptable battery lifetimes in future clinical oCI (*4*, *28*, *29*). Such efforts include achieving greater transduction rates and stronger expression by optimizing virus capsid, promoter and virus preparation, and better positioning of emitter(s) in scala tympani by arrays of micro-LEDs or waveguides (*29*). Our optical modeling indicated that placing an "ideal emitter" into scala tympani might markedly lower the energy required. Moreover, we expect that the higher energy requirements of the oCI due to the larger number of stimulation channels compared to eCI can be offset by lower rates of stimulation closer to the physiological SGN firing rates (*24*).

Studies of acoustically and optogenetically guided avoidance behavior in the shuttlebox indicated that acoustic percepts were formed with both modes of stimulation of the auditory pathway (sound and light). Immediate transfer of optogenetically trained behavior to acoustic stimulation was observed in all five gerbils investigated, whereas the opposite (transfer of acoustically induced behavior to optogenetic stimulation) was found for one of four acoustically trained, subsequently deafened, and oCI-implanted gerbils. By combining bilateral deafening by intracochlear kanamycin injection with chronic oCI, our results suggest that restoration of auditory function might be achieved with oCI.

Together, the results of our present study demonstrate the feasibility of optogenetic activation of the auditory system after AAV-CatCh transduction in SGNs in adult gerbils. We find good temporal precision

of optogenetically driven spiking in CatCh-expressing SGNs. Activity propagates up to AI. Furthermore, acoustic perception was confirmed in behavioral experiments with hearing and deaf animals. Our work increases the viability of cochlear optogenetics as an alternative hearing restoration technology and lays the foundation for in depth preclinical research.

Next to the far from complete viral transduction of the spiral ganglion and the employment of CatCh, which has a relatively slow deactivation, our study was limited by the use of oCIs based on single optical fibers with nonideal light projection onto SGNs. Our ray tracing model supports the expected potential for more spatially confined stimulation of SGNs when choosing appropriate positioning of emitters. Next steps of developing oCIs toward clinical application should include studies of spectral resolution combining appropriate multichannel stimulation-like waveguide array-based or micro-LED–based multichannel oCIs with electrophysiological and/or psychophysical studies of frequency and/or emitter discrimination (*29*). Such investigation of the cochlear spread of excitation with more realistic oCIs will help to determine the number of independently usable stimulation channels of future oCIs.

MATERIALS AND METHODS

Study design

We aimed to investigate optogenetic viral constructs to transduce SGNs in an adult rodent model for their potential for optogenetic hearing restoration. Animals transduced with a suitable construct were further investigated with physiological, immunohistochemical, imaging, and behavioral methods.

Statistical analysis

All data shown in the figures are expressed as mean ± SD, unless stated otherwise. Unless noted otherwise, an α level of 0.05 was considered significant. For SGN recordings, the presence of two subpopulations of SGNs was confirmed using Akaike's information criterion computed on the number of spike per pulse in response to 10-Hz light pulse train. Significance of different cutoff frequencies in these subpopulations was confirmed using the Mann-Whitney *U* test. Vector strength of SGNs was checked for significance using the Rayleigh criterion. If the Rayleigh statistic *L* was larger than 13.8, then the null hypothesis was rejected at the 0.001 significance level, and insignificant vector strengths were set to 0. For oABRs, an independent two-sample *t* test was used to analyze potential threshold differences of optically evoked ABRs in acute measurements versus chronically implanted animals. The relation between oABR amplitude and YFP-expressing SGNs was analyzed using simple linear regression. For behavior, because the behavioral output of an animal in the shuttlebox (compartment change/no compartment change) is a categorical one, response rates for nontarget and target trails for each animal were compared against each other using a chi-square test ($P < 0.01$) to determine significant performance. For auditory cortex recordings, threshold differences for optical stimulation of auditory cortex units tuned to low (1 to 8 kHz) and high (8 to 32 kHz) frequencies were analyzed using a one-sided independent two-sample *t* test. The exact number of animals contributing to each experiment is listed in table S1. Raw data for graphs containing an animal *n* lower than 20 are given in table S2. Statistical analyses were performed using MATLAB R2016a, R 3.4.4, and Python 3.6.

SUPPLEMENTARY MATERIALS

www.sciencetranslationalmedicine.org/cgi/content/full/10/449/eaao0540/DC1

Methods

Fig. S1. Effects of postnatal transfection of SGNs in adult Mongolian gerbils using the opsins Chronos and CatCh.

Fig. S2. SGN density of AAV-injected but CatCh-negative animals.

Fig. S3. oABRs: Dependence on stimulus intensity, rate, and duration—relationship to fraction of CatCh-expressing SGNs.

Fig. S4. Amplitude and latency comparison between aABRs and oABRs.

Fig. S5. Single auditory nerve fiber responses to acoustic click trains.

Fig. S6. oABR amplitudes and thresholds in chronically implanted gerbils.

Fig. S7. Determination of fiber position with three-dimensional x-ray tomography.

Fig. S8. Optical thresholds for AI single units with high versus low BFs.

Fig. S9. Estimating the spread of excitation using Monte Carlo ray tracing.

Fig. S10. Shuttlebox location detection algorithm.

Table S1. Number of animals used for each experiment.

Table S2. Raw data for graphs containing an animal *n* lower than 20.

References (*30*–*48*)

REFERENCES AND NOTES

1. World Health Organization (WHO), *Primary Ear and Hearing Care Training Resource* (WHO, 2006).
2. B. S. Wilson, M. F. Dorman, Cochlear implants: Current designs and future possibilities. *J. Rehabil. Res. Dev.* **45**, 695–730 (2008).
3. J. C. Middlebrooks, J. A. Bierer, R. L. Snyder, Cochlear implants: The view from the brain. *Curr. Opin. Neurobiol.* **15**, 488–493 (2005).
4. F.-G. Zeng, S. Rebscher, W. Harrison, X. Sun, H. Feng, Cochlear implants: System design, integration and evaluation. *IEEE Rev. Biomed. Eng.* **1**, 115–142 (2008).
5. A. Kral, R. Hartmann, D. Mortazavi, R. Klinke, Spatial resolution of cochlear implants: The electrical field and excitation of auditory afferents. *Hear. Res.* **121**, 11–28 (1998).
6. J. C. Middlebrooks, R. L. Snyder, Auditory prosthesis with a penetrating nerve array. *J. Assoc. Res. Otolaryngol.* **8**, 258–279 (2007).
7. R. V. Shannon, Multichannel electrical stimulation of the auditory nerve in man. II. Channel interaction. *Hear. Res.* **12**, 1–16 (1983).
8. L. M. Friesen, R. V. Shannon, D. Baskent, X. Wang, Speech recognition in noise as a function of the number of spectral channels: Comparison of acoustic hearing and cochlear implants. *J. Acoust. Soc. Am.* **110**, 1150–1163 (2001).
9. G. S. Donaldson, H. A. Kreft, L. Litvak, Place-pitch discrimination of single-versus dual-electrode stimuli by cochlear implant users (L). *J. Acoust. Soc. Am.* **118**, 623–626 (2005).
10. J. L. Pinyon, S. F. Tadros, K. E. Froud, A. C. Y. Wong, I. T. Tompson, E. N. Crawford, M. Ko, R. Morris, M. Klugmann, G. D. Housley, Close-field electroporation gene delivery using the cochlear implant electrode array enhances the bionic ear. *Sci. Transl. Med.* **6**, 233ra54 (2014).
11. C.-P. Richter, S. M. Rajguru, A. I. Matic, E. L. Moreno, A. J. Fishman, A. M. Robinson, E. Suh, J. T. Walsh Jr., Spread of cochlear excitation during stimulation with pulsed infrared radiation: Inferior colliculus measurements. *J. Neural Eng.* **8**, 056006 (2011).
12. V. H. Hernandez, A. Gehrt, K. Reuter, Z. Jing, M. Jeschke, A. M. Schulz, G. Hoch, M. Bartels, G. Vogt, C. W. Garnham, H. Yawo, Y. Fukazawa, G. J. Augustine, E. Bamberg, S. Kügler, T. Salditt, L. de Hoz, N. Strenzke, T. Moser, Optogenetic stimulation of the auditory pathway. *J. Clin. Invest.* **124**, 1114–1129 (2014).
13. T. Mager, P. G. Wood, E. Bamberg, Optogenetic control of Ca^{2+} and voltage-dependent large conductance (BK) potassium channels. *J. Mol. Biol.* **429**, 911–921 (2017).
14. S. Kleinlogel, K. Feldbauer, R. E. Dempski, H. Fotis, P. G. Wood, C. Bamann, E. Bamberg, Ultra light-sensitive and fast neuronal activation with the Ca^{2+}-permeable channelrhodopsin CatCh. *Nat. Neurosci.* **14**, 513–518 (2011).
15. N. C. Klapoetke, Y. Murata, S. S. Kim, S. R. Pulver, A. Birdsey-Benson, Y. K. Cho, T. K. Morimoto, A. S. Chuong, E. J. Carpenter, Z. Tian, J. Wang, Y. Xie, Z. Yan, Y. Zhang, B. Y. Chow, B. Surek, M. Melkonian, V. Jayaraman, M. Constantine-Paton, G. K.-S. Wong, E. S. Boyden, Independent optical excitation of distinct neural populations. *Nat. Methods* **11**, 338–346 (2014).
16. A. E. Hight, E. D. Kozin, K. Darrow, A. Lehmann, E. Boyden, M. C. Brown, D. J. Lee, Superior temporal resolution of Chronos versus channelrhodopsin-2 in an optogenetic model of the auditory brainstem implant. *Hear. Res.* **322**, 235–241 (2015).
17. W. Chen, N. Jongkamonwiwat, L. Abbas, S. J. Eshtan, S. L. Johnson, S. Kuhn, M. Milo, J. K. Thurlow, P. W. Andrews, W. Marcotti, H. D. Moore, M. N. Rivolta, Restoration of auditory evoked responses by human ES-cell-derived otic progenitors. *Nature* **490**, 278–282 (2012).
18. A. Huet, C. Batrel, Y. Tang, G. Desmadryl, J. Wang, J.-L. Puel, J. Bourien, Sound coding in the auditory nerve of gerbils. *Hear. Res.* **338**, 32–39 (2016).

19. M. Bartels, V. H. Hernandez, M. Krenkel, T. Moser, T. Salditt, Phase contrast tomography of the mouse cochlea at microfocus x-ray sources. *Appl. Phys. Lett.* **103**, 083703 (2013).
20. H. Schulze, H. Scheich, Discrimination learning of amplitude modulated tones in Mongolian gerbils. *Neurosci. Lett.* **261**, 13–16 (1999).
21. H. Hessel, M. Walger, S. Ernst, A. Foerst, H. von Wedel, H.-D. Klünter, W. Walkowiak, A method for the induction of a cochlea-specific auditory deprivation in the gerbil (Meriones unguiculatus). *ORL* **60**, 61–66 (1998).
22. W. Liu, R. L. Davis, Calretinin and calbindin distribution patterns specify subpopulations of type I and type II spiral ganglion neurons in postnatal murine cochlea. *J. Comp. Neurol.* **522**, 2299–2318 (2014).
23. R. Hallworth, R. F. Ludueña, Differential expression of β tubulin isotypes in the adult gerbil cochlea. *Hear. Res.* **148**, 161–172 (2000).
24. M. C. Liberman, Auditory-nerve response from cats raised in a low-noise chamber. *J. Acoust. Soc. Am.* **63**, 442–455 (1978).
25. J. A. Cardin, M. Carlén, K. Meletis, U. Knoblich, F. Zhang, K. Deisseroth, L.-H. Tsai, C. I. Moore, Targeted optogenetic stimulation and recording of neurons in vivo using cell-type-specific expression of Channelrhodopsin-2. *Nat. Protoc.* **5**, 247–254 (2010).
26. X. Han, In vivo application of optogenetics for neural circuit analysis. *ACS Chem. Neurosci.* **3**, 577–584 (2012).
27. L. A. Johnson, C. C. Della Santina, X. Wang, Selective neuronal activation by cochlear implant stimulation in auditory cortex of awake primate. *J. Neurosci.* **36**, 12468–12484 (2016).
28. C. M. Zierhofer, I. J. Hochmair-Desoyer, E. S. Hochmair, Electronic design of a cochlear implant for multichannel high-rate pulsatile stimulation strategies. *IEEE Trans. Rehabil. Eng.* **3**, 112–116 (1995).
29. C. Goßler, C. Bierbrauer, R. Moser, M. Kunzer, K. Holc, W. Pletschen, K. Köhler, J. Wagner, M. Schwaerzle, P. Ruther, O. Paul, J. Neef, D. Keppeler, G. Hoch, T. Moser, U. T. Schwarz, GaN-based micro-LED arrays on flexible substrates for optical cochlear implants. *J. Phys. D. Appl. Phys.* **47**, 205401 (2014).
30. J. Bourien, Y. Tang, C. Batrel, A. Huet, M. Lenoir, S. Ladrech, G. Desmadryl, R. Nouvian, J.-L. Puel, J. Wang, Contribution of auditory nerve fibers to compound action potential of the auditory nerve. *J. Neurophysiol.* **112**, 1025–1039 (2014).
31. J. M. Goldberg, P. B. Brown, Response of binaural neurons of dog superior olivary complex to dichotic tonal stimuli: Some physiological mechanisms of sound localization. *J. Neurophysiol.* **32**, 613–636 (1969).
32. C. M. Hillery, P. M. Narins, Frequency and time domain comparison of low-frequency auditory fiber responses in two anuran amphibians. *Hear. Res.* **25**, 233–248 (1987).
33. H. Thomas, J. Tillein, P. Heil, H. Scheich, Functional organization of auditory cortex in the mongolian gerbil (*Meriones unguiculatus*). I. Electrophysiological mapping of frequency representation and distinction of fields. *Eur. J. Neurosci.* **5**, 882–897 (1993).
34. P. V. Watkins, D. L. Barbour, Rate-level responses in awake marmoset auditory cortex. *Hear. Res.* **275**, 30–42 (2011).
35. C. Vogl, I. Panou, G. Yamanbaeva, C. Wichmann, S. J. Mangosing, F. Vilardi, A. A. Indzhykulian, T. Pangršič, R. Santarelli, M. Rodriguez-Ballesteros, T. Weber, S. Jung, E. Cardenas, X. Wu, S. M. Wojcik, K. Y. Kwan, I. del Castillo, B. Schwappach, N. Strenzke, D. P. Corey, S.-Y. Lin, T. Moser, Tryptophan-rich basic protein (WRB) mediates insertion of the tail-anchored protein otoferlin and is required for hair cell exocytosis and hearing. *EMBO J.* **35**, 2536–2552 (2016).
36. C. A. Schneider, W. S. Rasband, K. W. Eliceiri, NIH image to ImageJ: 25 years of image analysis. *Nat. Methods* **9**, 671–675 (2012).
37. W. van Aarle, W. J. Palenstijn, J. De Beenhouwer, T. Altantzis, S. Bals, K. J. Batenburg, J. Sijbers, The ASTRA toolbox: A platform for advanced algorithm development in electron tomography. *Ultramicroscopy* **157**, 35–47 (2015).
38. W. van Aarle, W. J. Palenstijn, J. Cant, E. Janssens, F. Bleichrodt, A. Dabravolski, J. De Beenhouwer, K. J. Batenburg, J. Sijbers, Fast and flexible x-ray tomography using the ASTRA toolbox. *Opt. Express* **24**, 25129–25147 (2016).
39. P. van der Zee, "Measurement and modelling of the optical properties of human tissue in the near infrared," thesis, University College London (1992).
40. J. Steinbrink, "Nahinfrarotspektroskopie am Kopf des Erwachsenen mit Pikosekunden-Zeitauflösung", thesis, Freie Universität Berlin (2000).
41. N. Yavari, S. Andersson-Engels, J. Sorensen Dam, J. Antonsson, K. Wardell, "Measurements of Optical Properties of Pig Brain Tissue in vitro Using a Novel Compact Device," in *Novel Optical Instrumentation for Biomedical Applications II*, C. Depeursinge, Ed., vol. 5864 of Proc. SPIE (Optical Society of America, 2005); https://doi.org/10.1364/ECBO.2005.MG4.
42. N. Lue, J. Bewersdorf, M. D. Lessard, K. Badizadegan, R. R. Dasari, M. S. Feld, G. Popescu, Tissue refractometry using Hilbert phase microscopy. *Opt. Lett.* **32**, 3522–3524 (2007).
43. A. O. Ugnell, P. Å. Öberg, The optical properties of the cochlear bone. *Med. Eng. Phys.* **19**, 630–636 (1997).
44. F. Bevilacqua, D. Piguet, P. Marquet, J. D. Gross, B. J. Tromberg, C. Depeursinge, In vivo local determination of tissue optical properties: Applications to human brain. *Appl. Opt.* **38**, 4939–4950 (1999).
45. M. H. Niemz, *Laser-Tissue Interactions: Fundamentals and Applications* (Springer, 2007).
46. S. L. Jacques, Optical properties of biological tissues: A review. *Phys. Med. Biol.* **58**, R37–R61 (2013).
47. S. Haleh, G. Hirac, P. Frédéric, Optical properties of mice skull bone in the 455- to 705-nm range. *J. Biomed. Opt.* **22**, 010503 (2017).
48. V. V. Tuchin, *Tissue Optics: Light Scattering Methods and Instruments for Medical Diagnosis* (SPIE Press, 2007); http://spie.org/Publications/Book/2175698.

Acknowledgments: We thank M. Rivolta for teaching us the modiolar injection. We thank K. Bodensiek for devising the optical model. We thank M. Töpperwien and T. Salditt for enabling the x-ray tomography. We also thank S. Gerke, J. Paech, C. Senger-Freitag, and P. Wenig for expert technical assistance. **Funding:** This work was funded by the European Research Council under the European Union's Horizon 2020 Research and Innovation Programme (grant agreement no. 670759 and advanced grant "OptoHear" to T.M.) and was further supported by grants from the German Research Foundation through the Collaborative Research Center 889 (project research rotation of C.W.), the Center for Nanoscale Microscopy and Molecular Physiology of the Brain and the Leibniz Program (to T.M.), and a grant from the Georgius Agricola Foundation Ruhr (to C.W. and S. Dazert). A.D. is a fellow of the German Academic Scholarship Foundation. C.V. is a Creutzfeldt fellow of the Elisabeth and Helmut Uhl Foundation. **Author contributions:** C.W., A.D., M.J., and T.M. designed the study. C.W. performed AAV injections, immunohistochemistry, oABR/aABR recordings, and SGN recordings in the early phase of the project. C.W and M.J. performed recordings from single AC units. A.D. performed AAV injections, chronic oCI, oABR/aABR recordings, shuttlebox, and deafening experiments. A.D. and M.J. designed behavioral experiments. A.H. performed AAV injections and recordings from single SGNs that are presented in this manuscript. D.K. performed x-ray tomography. C.J.D.-A. performed the Monte Carlo modeling of optical rays. C.V. performed the immunohistochemistry of whole-mount organs of Corti. G.H. and M.J. designed the shuttlebox and other hard/software. All authors analyzed data and prepared the manuscript. **Competing interests:** The authors declare that they have no competing interests. **Data and materials availability:** All data associated with this study are in the paper and/or the Supplementary Materials.

Submitted 9 June 2017
Resubmitted 17 November 2017
Accepted 19 June 2018
Published 11 July 2018
10.1126/scitranslmed.aao0540

Citation: C. Wrobel, A. Dieter, A. Huet, D. Keppeler, C. J. Duque-Afonso, C. Vogl, G. Hoch, M. Jeschke, T. Moser, Optogenetic stimulation of cochlear neurons activates the auditory pathway and restores auditory-driven behavior in deaf adult gerbils. *Sci. Transl. Med.* **10**, eaao0540 (2018).

Science Translational Medicine

Optogenetic stimulation of cochlear neurons activates the auditory pathway and restores auditory-driven behavior in deaf adult gerbils

Christian Wrobel, Alexander Dieter, Antoine Huet, Daniel Keppeler, Carlos J. Duque-Afonso, Christian Vogl, Gerhard Hoch, Marcus Jeschke and Tobias Moser

Sci Transl Med **10**, eaao0540.
DOI: 10.1126/scitranslmed.aao0540

Listening to light

Cochlear implants rely on electrical stimulation of the auditory nerve to provide a sense of sound to a person with severe hearing loss. However, the resolution of complex sounds is limited by the spreading of the current around the electrode. Wrobel *et al*. leveraged optogenetics to develop an optical cochlear implant that uses light for spatially and temporally precise stimulation of the auditory nerve in deaf adult gerbils. After virus-mediated expression of a light-sensitive protein in cochlear neurons, the optical implant was able to stimulate the auditory pathway and restored auditory-driven behavior in deaf gerbils. Further studies testing the resolution potential of optical cochlear implants are warranted.

Science Translational Medicine (ISSN 1946-6242) is published by the American Association for the Advancement of Science, 1200 New York Avenue NW, Washington, DC 20005.